Journal of Pharmaceutical Analysis 14 (2024) 100910

Contents lists available at ScienceDirect

Journal of Pharmaceutical Analysis

journal homepage: www.elsevier.com/locate/jpa

Original article

Integrated spatial metabolomics and transcriptomics decipher the hepatoprotection mechanisms of wedelolactone and demethylwedelolactone on non-alcoholic fatty liver disease

Panpan Chen [a, b, 1], Zihan Zhu [a, b, c, 1], Haoyuan Geng [b], Xiaoqing Cui [a, b], Yuhao Han [b], Lei Wang [b], Yaqi Zhang [b], Heng Lu [a, b], Xiao Wang [a, b], Yun Zhang [d, **], Chenglong Sun [a, b, *]

[a] Key Laboratory for Natural Active Pharmaceutical Constituents Research in Universities of Shandong Province, School of Pharmaceutical Sciences, Qilu University of Technology (Shandong Academy of Sciences), Jinan, 250014, China
[b] Key Laboratory for Applied Technology of Sophisticated Analytical Instruments of Shandong Province, Shandong Analysis and Test Center, Qilu University of Technology (Shandong Academy of Sciences), Jinan, 250014, China
[c] School of Pharmacy, Shandong University of Traditional Chinese Medicine, Jinan, 250355, China
[d] Biology Institute, Qilu University of Technology (Shandong Academy of Sciences), Jinan, 250103, China

ARTICLE INFO

Article history:
Received 27 July 2023
Received in revised form
12 November 2023
Accepted 27 November 2023
Available online 29 November 2023

Keywords:
Spatial metabolomics
Transcriptomics
Non-alcoholic fatty liver disease
Wedelolactone
Demethylwedelolactone

ABSTRACT

Eclipta prostrata L. has been used in traditional medicine and known for its liver-protective properties for centuries. Wedelolactone (WEL) and demethylwedelolactone (DWEL) are the major coumarins found in *E. prostrata* L. However, the comprehensive characterization of these two compounds on non-alcoholic fatty liver disease (NAFLD) still remains to be explored. Utilizing a well-established zebrafish model of thioacetamide (TAA)-induced liver injury, the present study sought to investigate the impacts and mechanisms of WEL and DWEL on NAFLD through integrative spatial metabolomics with liver-specific transcriptomics analysis. Our results showed that WEL and DWEL significantly improved liver function and reduced the accumulation of fat in the liver. The biodistributions and metabolism of these two compounds in whole-body zebrafish were successfully mapped, and the discriminatory endogenous metabolites reversely regulated by WEL and DWEL treatments were also characterized. Based on spatial metabolomics and transcriptomics, we identified that steroid biosynthesis and fatty acid metabolism are mainly involved in the hepatoprotective effects of WEL instead of DWEL. Our study unveils the distinct mechanism of WEL and DWEL in ameliorating NAFLD, and presents a "multi-omics" platform of spatial metabolomics and liver-specific transcriptomics to develop highly effective compounds for further improved therapy.

1. Introduction

The escalating prevalence of non-alcoholic fatty liver disease (NAFLD), affecting approximately 30% of the adult population globally, has turned it into the leading chronic liver disorder [1]. NAFLD is essentially attributed to metabolic dysfunction and can be characterized by the hepatic fat accumulation, which evolves from benign fatty liver to non-alcoholic steatohepatitis [2,3]. With ongoing liver damage, NAFLD often progresses to severe outcomes such as liver dysfunction and primary liver cancer, contributing to a marked increase in liver-related mortality [4,5]. NAFLD is also strongly associated with obesity [6], insulin resistance [7] and other metabolic diseases [8]. Despite the demand for NAFLD treatments continues to rise, currently no drugs have yet been approved, and the development of effective and affordable treatments for NAFLD is still challenging.

Eclipta prostrata L. is widely used in traditional medicines for its liver-tonifying properties across Asia, America and Africa [9,10], exhibiting favorable biological effects on diverse liver diseases caused by alcohol overdose [11], infectious agents [12], toxins damage [13], hepatic fibrosis [14], etc. Wedelolactone (WEL) and demethylwedelolactone (DWEL), the naturally occurring coumarins

* Corresponding author. Key Laboratory for Applied Technology of Sophisticated Analytical Instruments of Shandong Province, Shandong Analysis and Test Center, Qilu University of Technology (Shandong Academy of Sciences), Jinan, 250014, China.
** Corresponding author.
E-mail addresses: xiaohan_0818@163.com (Y. Zhang), chenglongsun1989@163.com (C. Sun).
[1] Both authors contributed equally to this work.

https://doi.org/10.1016/j.jpha.2023.11.017

in *Eclipta prostrata* L., are considered to be the predominant bioactive ingredients for its therapeutic properties. Not only for liver injury, WEL has also been reported to alleviate various metabolic disorders like hyperlipidemia and hyperglycaemia, potentially via the activation of AMP-activated protein kinase (AMPK)/peroxisome proliferator-activated receptor α (PPARα) to reduce lipids [15]. However, the specific impact and mechanisms of WEL in NAFLD remains inadequate, and there is still a lack of knowledge on the potential benefit of DWEL on NAFLD, leaving the uncertainty of whether the methyl group absence in DWEL contributes to the differences in biological processes compared to WEL.

As a vertebrate model organism, zebrafish (*Danio rerio*) exhibit various beneficial traits, making them a preferred choice in many major liver diseases [16–18]. Besides the superiorities of rapid development and cost-effectiveness, zebrafish also possess a high degree of physiological and genetic similarity to humans, especially regarding hepatic cellular composition, function, and the underlying cellular processes [19]. More remarkably, the liver-specific fluorescent transgenic lines allow for precise and direct *in vivo* visualization, accelerating the research of disease pathogenesis as well as the advancement of therapeutic strategies [20,21]. The multi-omics analysis, which can be utilized on zebrafish model, has been recognized as an increasingly powerful tool in liver disease research. The combination of metabolomics and transcriptomics stands out as particularly significant [22–24]. While the conventional metabolomics profiles reveal numerous metabolites alterations in these metabolic disorders, the spatial information is utterly lost after tissue homogenization. The spatial resolved metabolomics, which employs the mass spectrometry imaging (MSI) technique, enables the mapping of thousands of functional metabolites without labeling *in situ*. It also facilitates the characterization of drug distribution and metabolism in spheroids [25,26], cancer tissues and organs [27–29], prompting us to investigate the liver damage in zebrafish. Moreover, integrating spatial metabolomics with transcriptomics shall yield a great deal of differently expressed genes and metabolic pathways, bridging the gap between phenotype and genotype by converging two disparate data sets.

In our present study, we employed the transgenic zebrafish featuring liver-specific red fluorescence to construct the NAFLD model through thioacetamide (TAA) induction, and explored the impacts and the underlying mechanism of WEL and DWEL on NAFLD. The design of this study is shown in Scheme 1. We found that both WEL and DWEL could ameliorate metabolic disturbances caused by NAFLD, while WEL profoundly exerts its effects through the modulation of steroid biosynthesis and fatty acid metabolism. The integrative approach of spatial metabolomics and transcriptomics not only provides valuable insights into unravelling the intricate dynamics of metabolic remodeling in NAFLD, but also enhances our ability for the development of novel therapeutic strategies targeting related metabolic disorders.

2. Materials and methods

2.1. Reagents and chemicals

1,5-Diaminonaphthalene (1,5-DAN) was purchased from Shanghai Aladdin Bio-chemical Technology Co., Ltd (Shanghai, China). Acetonitrile (ACN) was afforded by Merck (Darmstadt, Germany). The indium tin oxide-coated slides were provided by Bruker Daltonics (Billerica, MA, USA). Superfrost Plus slides were purchased from ThermoFisher Scientific (Waltham, MA, USA). Wedelolactone (WEL) and demethylwedelolactone (DWEL) were both purchased from TargetMol (Boston, MA, USA), and dissolved in dimethyl sulfoxide (DMSO; Sigma, St. Louis, MO, USA). Thioacetamide (TAA) was obtained from Sigma.

2.2. Zebrafish maintenance

The transgenic zebrafish line Tg (lfabp10:DsRed), selectively expressing red fluorescent protein DsRed in liver [21], was sourced from Zebrafish Drug Screening Platform of Shandong Academy of Sciences (Jinan, China). The adult zebrafish were housed in an aquaculture facility with 14-h light and 10-h darkness photoperiod at 28 ± 0.5 °C. The embryos were maintained in E3 medium (5 mM NaCl, 0.17 mM KCl, 0.33 mM $CaCl_2$, 0.33 mM $MgSO_4$ and 0.0001% methylene blue) within the incubator at the same temperature and photoperiod. All the experimental procedures were carried out under the approval of the Biology Institute, Qilu University of Technology Animal Ethics Committee (Approval number: SWS20210315).

2.3. Hepatoprotective activity assay

The well-developed zebrafish larvae at 72 h post-fertilization (hpf) were randomly transferred to a 6-well plate with 20 larvae per well. To test the hepatoprotective activity of WEL and DWEL, zebrafish were treated with 10 mM TAA along with different

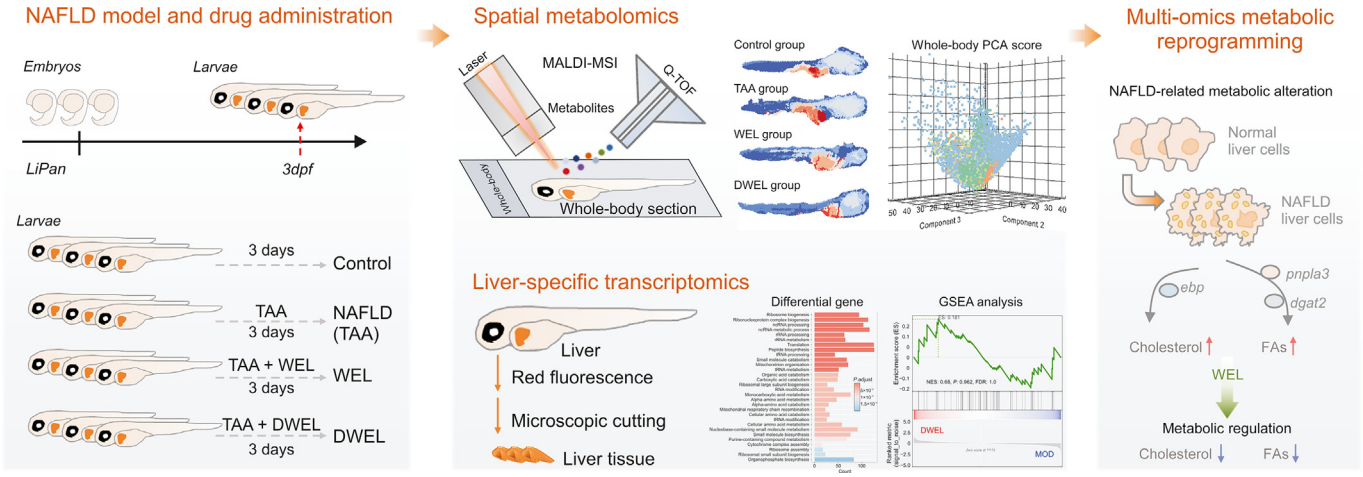

Scheme 1. The strategy of integrating spatial metabolomics and transcriptomics deciphers the hepatoprotection mechanisms of wedelolactone (WEL) and demethylwedelolactone (DWEL) on non-alcoholic fatty liver disease (NAFLD). TAA: thioacetamide; MALDI-MSI: matrix-assisted laser desorption/ionization-mass spectrometry imaging; Q-TOF: quadrupole time-of-flight; PCA: principal component analysis; GSEA: gene set enrichment analysis; MOD: model; FAs: fatty acids.

concentrations of WEL or DWEL (30 μM, 10 μM, and 3 μM). Those exposed solely to 10 mM TAA were served as the model group. The zebrafish maintained in fresh fish water without any treatment were utilized as the blank control. At 120 hpf, the larvae were anesthetized with tricaine (Sigma) and immobilized in 3% methylcellulose (Beyotime, Shanghai, China), and then were observed and photographed under the inverted fluorescent microscope (Olympus, Tokyo, Japan).

2.4. Oil red O staining

To prepare the oil red O working solution, 0.5 g of oil red O powder (Sigma) are fully dissolved in 100 mL isopropanol and stored at 4 °C in the dark. Before use, the stock solution was diluted with distilled water at the ratio of 3:2 (*V/V*), and then was thoroughly filtered through the 0.22 μm micropore filter to obtain the working solution without sediment. After treatment, zebrafish larvae were fixed in the 4% paraformaldehyde at 4 °C overnight, followed by dehydration in a sequential gradient of 25%, 50%, 75%, and 100% propylene glycol/phosphate-buffered saline (PBS) for 10 min respectively. The larvae were then stained with the oil red O working solution overnight at room temperature, and redehydrated in 100%, 75%, 50%, 25% propylene glycol/PBS. The pathological changes were observed using the stereomicroscope.

2.5. Biochemical analysis

The zebrafish larvae were gathered and washed in PBS three times, followed by homogenization in cold saline at a weight-to-volume ratio of 1:9. The homogenate was then centrifuged at 15,000 *g* for 15 min at 4 °C and the supernatant was retained and measured for protein concentration using the Bradford kit (Nanjing Jiancheng Bioengineering Institute, Nanjing, China). Following the manufacturer's kits and instructions, the activities or contents of aspartate transaminase (AST) and total triglyceride (TG) in the supernatant were detected.

2.6. Preparation of frozen sections of zebrafish

The whole body of zebrafish was embedded in optimal cutting temperature (OCT) compound and sectioned into continuous fifteen-micron tissue sections using a cryostat microtome (CryoStar NX50 NOVPD, Thermo, Bremen, Germany). For each zebrafish, one of the frozen sections was subjected to hematoxylin and eosin (H&E) staining, and two of the frozen sections were subjected to matrix-assisted laser desorption/ionization-mass spectrometry imaging (MALDI-MSI) analysis in positive and negative ion modes, respectively.

2.7. MALDI-MS imaging analysis

1,5-DAN was selected as the matrix for MALDI-MS imaging of zebrafish whole-body section. 2.5 mg/mL 1,5-DAN in ACN/H_2O (70:30, *V/V*) was sprayed onto the surface of zebrafish section by using a HTX TM-Sprayer™ (HTX Technologies, Carrboro, NC, USA). The flow rate of 1,5-DAN solution was set to 75 μL/min. Nozzle nitrogen pressure and temperature was set 10 psi and 55 °C, respectively. Fourteen cycles of 1,5-DAN solution were sprayed on zebrafish section, and the nozzle-to-slice distance was set to 4 cm. MALDI-MSI experiments were performed in the *m/z* range of 70–1,000 using a RapifleX MALDI Tissuetyper™ TOF/TOF MS (Bruker Daltonics). LasAtten value was optimized according to the ion intensities and mass resolutions of metabolites and lipids. Laser repetition rate was set to 5,000 Hz and the laser shots were set to 200. Ion source voltage 1 and ion source voltage 2 were set to 20 kV and 17.42 kV, respectively. The Lens voltage was set to 11.6 kV. The imaging resolution was 20 μm. The MS images were constructed using SCiLS Lab 2018b software (GmbH, Bremen, Germany). The ion intensities and *in situ* data analysis including principal component analysis, probabilistic latent semantic analysis, data-driven segmentation analysis was also calculated using SCiLS Lab 2018b software.

2.8. RNA sequencing analysis

The liver of the zebrafish was carefully dissected, and the total RNA was extracted using TRIzol reagent (ThermoFisher). The RNA integrity was evaluated utilizing the RNA Nano 6000 Assay Kit on the Bioanalyzer 2100 system (Agilent Technologies, Santa Clara, CA, USA). Then the cDNA library were constructed using Stranded mRNA LTSample Prep Kit (Illumina, Santa Clara, CA, USA) and sequenced on Illumina NovaSeq 6000 platform, which were conducted by OE Biotech Co., Ltd (Shanghai, China). The raw transcriptome data was processed using Trimmomatic [30] and the clean reads were mapped to the Danio rerio genome (assembly GRCz11) using HISAT2 [31]. DESeq2 R package was used to identify the differentially expressed genes (DEGs) among two comparison groups [32], with the threshold of P value < 0.05 and fold change >1.2 or fold change <0.8. Kyoto Encyclopedia of Genes and Genomes (KEGG) enrichment analysis of DEGs were performed by the cluster profile R package. Gene Set Enrichment Analysis (GSEA) was conducted using the OECloud tools (https://cloud.oebiotech.com) and single-sample GSEA (ssGSEA) was performed using GSVA R package [33].

2.9. Quantitative real-time PCR (qRT-PCR) assay

Total RNA was extracted using Spin Column Animal Total RNA Purification Kit (Sangon Biotech, Shanghai, China), and then were subjected to reverse transcription by AMeasy 1st Strand cDNA Synthesis Kit (Allmeek, Beijing, China). Next, qRT-PCR analysis was performed using 2× PerfectHS SYBR QPCR Mixture Kit (Allmeek). Specific primer information was shown in Supporting information Table S1. The relative mRNA levels of target genes were calculated by $2^{-\triangle\triangle Ct}$ method and β-actin was used as control for normalization.

2.10. Statistical analysis

Statistical analysis was conducted using GraphPad Prism Software (version 8.0, San Diego, CA, USA). All data were presented as mean ± standard deviation (SD). Student's *t*-test and one-way analysis of variance (ANOVA) followed by Dunnett's test were utilized for conducting comparative analysis of two groups and multiple groups, respectively. A P value below the threshold of 0.05 was considered statistically significant.

3. Results and discussion

3.1. The protective effects of WEL and DWEL in TAA-induced liver injury

To evaluate the potential hepatoprotective effects of WEL and DWEL, zebrafish larvae were exposed to TAA to induce the liver

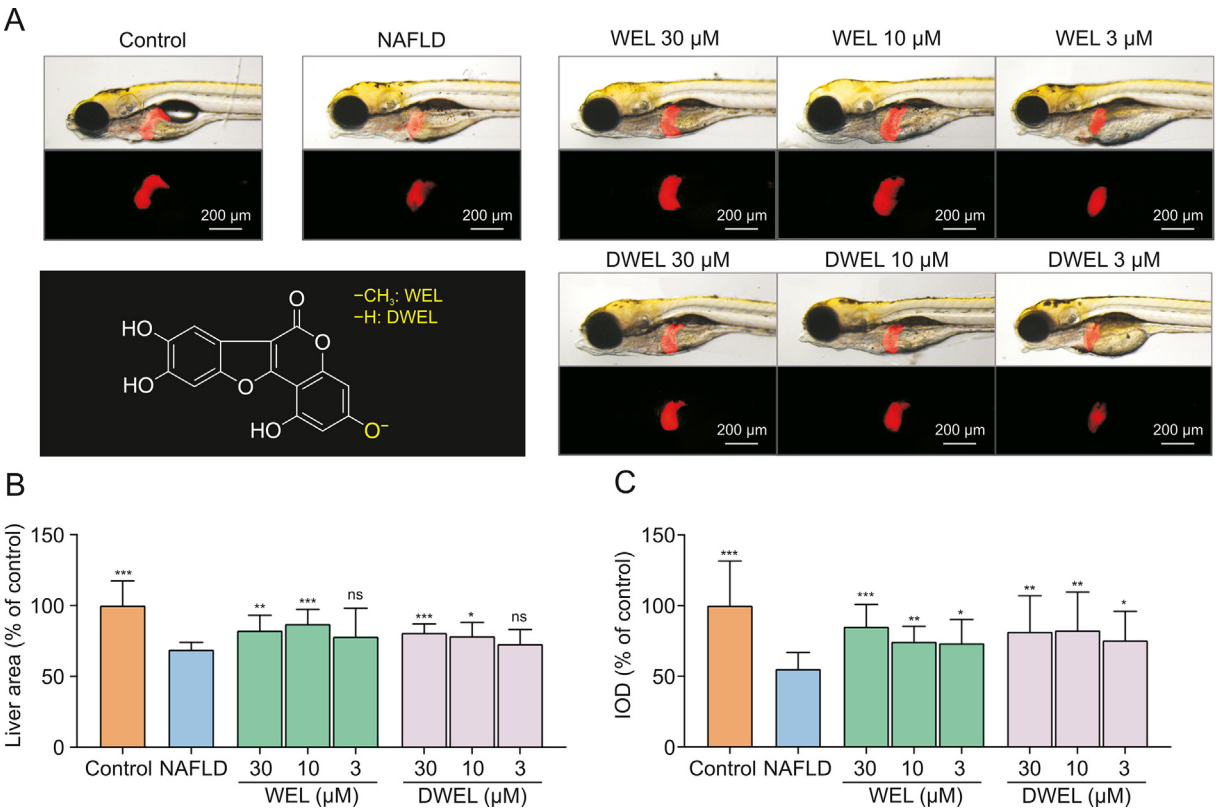

Fig. 1. Effects of wedelolactone (WEL) and demethylwedelolactone (DWEL) on thioacetamide (TAA)-damaged zebrafish larvae. (A) The structure of WEL and DWEL, and their hepatoprotection against TAA-damaged zebrafish larvae. (B) Quantification of liver area in each group. (C) Quantitative analysis of the liver fluorescence intensity. Data are presented as mean ± standard deviation (SD) ($n = 10$). $^{*}P < 0.05$, $^{**}P < 0.01$, $^{***}P < 0.001$, ns: no significance. NAFLD: non-alcoholic fatty liver disease; IOD: integrated optical density.

injury, and simultaneously treated with WEL or DWEL until 120 hdf. As shown in Fig. 1A, the TAA-treated group displayed a significant reduction in both liver size and fluorescent intensity when compared to the untreated control group. Notably, the liver area as well as the integrated optical density (IOD) were significantly increased when treated with WEL or DWEL (Figs. 1B and C), suggesting that both WEL and DWEL could ameliorate liver injury. Meanwhile, no visually pathological changes were observed in zebrafish treated with WEL or DWEL.

3.2. The suppression of WEL and DWEL on lipid accumulation in zebrafish liver

TAA is known to dysregulate the lipid metabolism of the liver, inducing lipid accumulation which promoted the impairment of the hepatocyte function. To verify the effect of WEL and DWEL on lipid accumulation, zebrafish larvae were subjected to red oil O staining. Obviously, TAA treatment leads to higher levels of lipids than the control (Fig. 2), implying that TAA caused NAFLD in zebrafish. Less lipids were found in WEL or DWEL-treated zebrafish in a dose-dependent manner, which suggested that WEL or DWEL treatment reduced lipids accumulation in zebrafish liver (Figs. 2A and B). The yolk sac of the zebrafish, 70% of which is neutral lipid primarily metabolized in liver, is regarded as an important manifestation of liver function [34,35]. According to the results in Fig. 2C, zebrafish treated with TAA showed an increase of yolk sac area, indicating a delayed absorption and live injury. Strikingly, both WEL and DWEL could promote the absorption of the yolk and lead to a decrease of the yolk sac area, in line with the results of the red oil O staining. We also found that WEL and DWEL reduce the level of aspartate aminotransferase (AST) and total triglyceride (TG) that was elevated by TAA induction (Fig. S1). Taken together, WEL and DWEL treatment alleviated lipids accumulation in zebrafish liver.

3.3. Imaging the spatial distributions of WEL and DWEL and their metabolites in whole-body zebrafish sections

Mass spectrometry imaging enables simultaneous characterization of the spatial distributions and relative contents of drugs and their metabolites in heterogeneous biological tissues. A better understanding of the biodistribution and metabolism of the drugs is certain to advance the research on their safety and efficacy. In this study, we successfully mapped the spatial distributions of WEL and DWEL in different organs of zebrafish in whole-body zebrafish sections. Moreover, we can also detect and image the phase I and phase II metabolites of WEL and DWEL in zebrafish whole-body sections.

Fig. 3A illustrates the metabolites of WEL identified in zebrafish. In the WEL group, WEL underwent demethylation to generate DWEL, and we also detected methylation metabolites of WEL. In addition, we found that WEL, as well as DWEL and methylated WEL, can continue to undergo sulfation and glucuronidation phase II metabolic reactions in zebrafish (Fig. 3A). This finding is consistent with the previously reported metabolism of WEL in rats [36]. More notably, we identified the sulfated-glucosidated metabolites of WEL, DWEL, and methylated WEL *in vivo*, which, to our knowledge, has not been reported previously. A total of fourteen metabolites of WEL were identified in zebrafish. Fig. 3B shows the MS images of WEL and its fourteen metabolites in different organs of zebrafish. The results indicate that WEL and its phase I and phase II metabolites mainly distributed in the liver and intestines, while their contents in other organs such as the brain, muscles, and eyes are

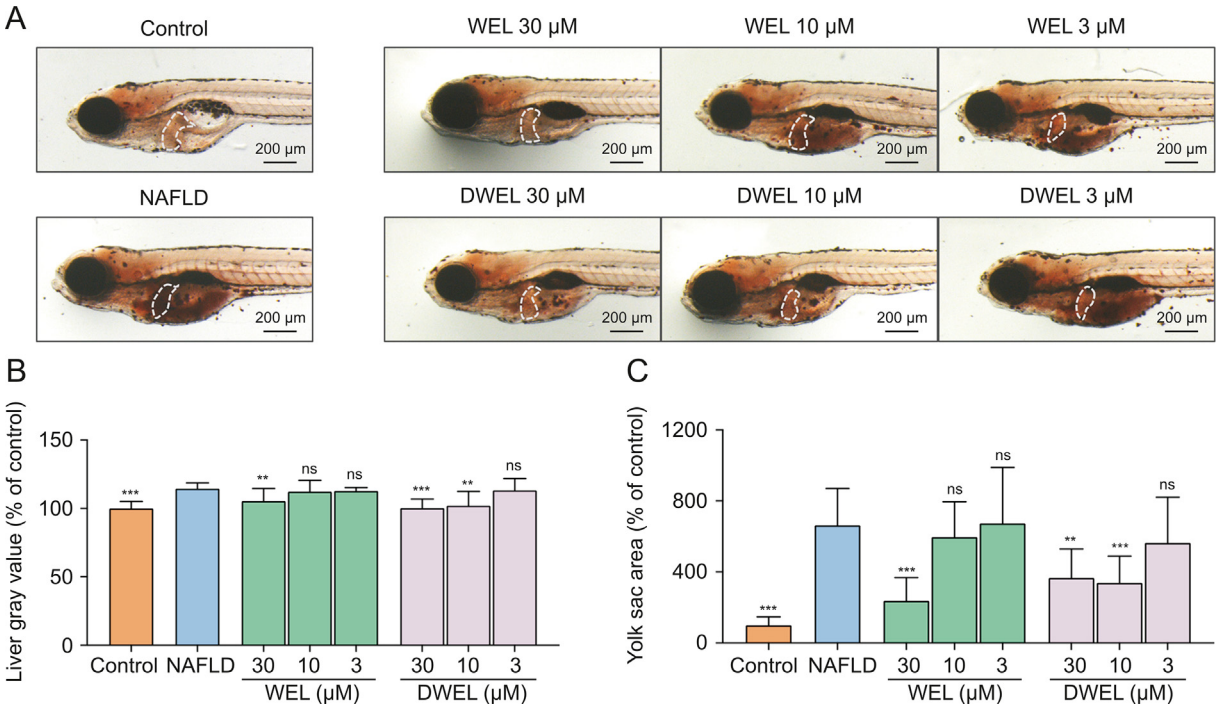

Fig. 2. Effects of wedelolactone (WEL) and demethylwedelolactone (DWEL) on lipids accumulation in zebrafish liver. (A) Oil red O staining of zebrafish larvae. (B) Staining quantitation of zebrafish liver of each group. (C) Quantitative analysis of yolk area in zebrafish larvae. Data are presented as mean ± standard deviation (SD) ($n = 10$). $^{*}P < 0.05$, $^{**}P < 0.01$, $^{***}P < 0.001$, ns: no significance. The white dotted lines outline the liver area.

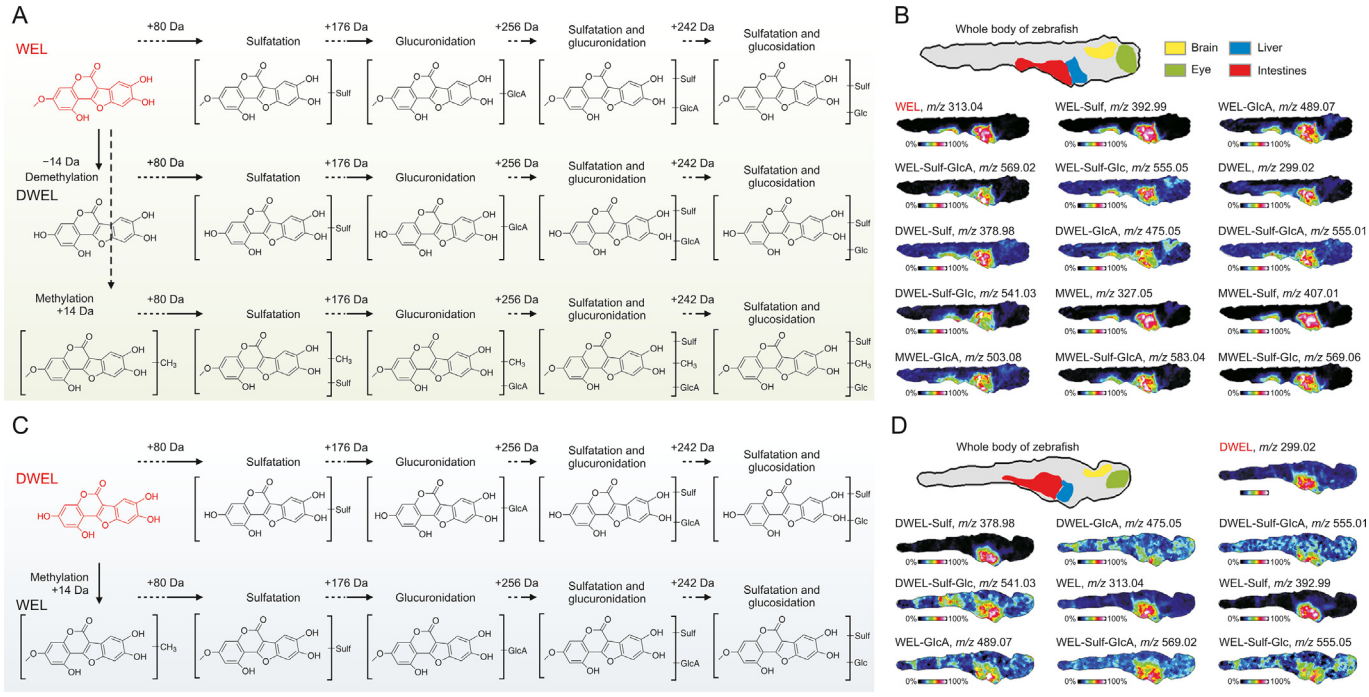

Fig. 3. The metabolism and spatial signatures of wedelolactone (WEL) and demethylwedelolactone (DWEL) in zebrafish. (A) Metabolism pathway of WEL and the structural inferences of its metabolites. (B) Mass spectrometry (MS) images depicting the spatial distribution of WEL and its metabolites in zebrafish whole-body section. (C) Metabolism pathway of DWEL and the structural inferences of its metabolites. (D) MS images depicting the spatial distribution of DWEL and its metabolites in zebrafish. WEL-Sulf: sulfated wedelolactone; WEL-GlcA: glucuronidated wedelolactone; WEL-Sulf-GlcA: sulfated-glucuronidated wedelolactone; WEL-Sulf-Glc: sulfated-glucosidated wedelolactone; DWEL-Sulf: sulfated demethylwedelolactone; DWEL-GlcA: glucuronidated demethylwedelolactone; DWEL-Sulf-GlcA: sulfated-glucuronidated demethylwedelolactone; DWEL-Sulf-Glc: sulfated-glucosidated demethylwedelolactone; MWEL: methylated wedelolactone; MWEL-Sulf: methylated and sulfated wedelolactone; MWEL-GlcA: methylated and glucuronidated wedelolactone; MWEL-Sulf-GlcA: methylated, sulfated and glucuronidated wedelolactone; MWEL-Sulf-Glc: methylated, sulfated and glucosidated wedelolactone.

very low. This suggests that the liver and intestines are the main metabolic organs of WEL in zebrafish, and may also be the main target organs for WEL to exert its biological effects.

In the DWEL group (Fig. 3C), we found that DWEL could first undergo methylation in zebrafish to generate methylated DWEL. Afterwards, DWEL and methylated DWEL can be further combined with sulfuric acid and glucuronic acid with 80 Da and 176 Da mass shifts. In addition, we discovered that one molecule of DWEL and methylated DWEL can be combined with one molecule of sulfuric acid and one molecule of glucuronide to undergo both sulfation and glucuronidation reactions with 256 Da mass shift. And, one molecule of DWEL and methylated DWEL can be combined with one molecule of sulfuric acid and one molecule of glucose to undergo both sulfation and glucosidation reactions with 242 Da mass shift. This analysis also represents the first characterization of DWEL metabolism *in vivo*. As with WEL, the parent compound and metabolites of DWEL predominantly characterized within the liver and gut, whereas the glucosidated or glucuronidated metabolites of DWEL were also detected in other organs throughout the entire body (Fig. 3D). Table S2 shows the high performance liquid chromatography-high resolution mass spectrometry (HPLC-HR-MS) data of WEL and DWEL metabolites, and all the metabolites were verified using exact molecular weights and a mass accuracy of less than 5 ppm. We further carried out HPLC-HR-MS/MS analysis on these target compounds and the structure-specific pattern ions of the target analyte were used for further identification (Figs. S2–11). Taken together, our study highlights the metabolism of WEL and DWEL in zebrafish, implying that zebrafish possess a complete metabolic organ system and similar metabolic enzyme systems as humans, providing an ideal model for drug metabolism research.

3.4. Spatial metabolomics highlights the metabolic modulation by WEL and DWEL on NAFLD

We further carried out spatial metabolomics on zebrafish whole-body sections to explore the metabolic alterations during the development of NAFLD and the metabolic modulations by WEL and DWEL on NAFLD. No significant variations were discerned in terms of the zebrafish size and the H&E staining results among the control, NAFLD model, WEL, and DWEL groups (Fig. 4A). Then, we performed data-driven whole-body segmentation analysis based on the region-specific metabolite fingerprints (Fig. 4B). In the whole-body segmentation map, different regions with similar metabolite profiles were grouped together and given a specific color. It was found that all the zebrafish whole-body sections presented significant color diversity, and the liver and intestines regions were assigned as hot red color and other organs were more often assigned as cool blue color. More interestingly, we found that the liver region was given a more intense red compared to the control, WEL, and DWEL groups (Fig. 4B). This result suggests that significant metabolic reprogramming occurred in the liver tissue during the development of NAFLD and its metabolic profile gradually returned to normal after the administration of WEL and DWEL.

Given the limitations of zebrafish larvae size, profiling of NAFLD-related metabolic alteration has traditionally been performed on whole zebrafish larvae, which has resulted in the inability to accurately obtain organ-specific metabolic signatures. The introduction of MSI into metabolomics offered an insight approach to precisely characterize NAFLD related metabolic alterations. As shown in Figs. 4C and D, when we extracted the metabolic profiles on zebrafish whole-body section for principal component analysis (PCA) and probabilistic latent semantic analysis (PLSA), the metabolic features of the control, NAFLD model, WEL, and DWEL groups were difficult to be identified and distinguished. However, if liver-specific metabolic profiles were extracted on liver region of zebrafish whole-body section for PLSA analysis, we discovered obvious clustering and grouping trends for control, NAFLD model, WEL, and DWEL groups (Fig. 4E). Overall, liver metabolism was significantly altered in the NAFLD group compared to the control group, while the metabolic characteristics of the WEL and DWEL groups were closer to those of the control group (arrows in Fig. 4E), which would suggest that WEL and DWEL were able to partially inhibit the metabolic alterations caused by NAFLD. This also echoes our previous finding that WEL and DWEL can prevent or ameliorate liver injury.

We proceeded to screen and image the discriminatory metabolites modulated by WEL and DWEL on NAFLD. As a primary participant in systemic nitrogen metabolism and energy metabolism, glutamine exhibited disrupted metabolic homeostasis within NAFLD, showing a marked increase of its expression. This condition, however, was notably mitigated by the introduction of WEL and DWEL (Fig. 4F). Catalyzed by glutaminase, glutamine can be metabolized into glutamate, which subsequently enters the TCA cycle for energy production or is employed for glutathione synthesis [37]. Correspondingly, we revealed a similar trend in the levels of glutamate and glutathione (Figs. 4G and H). Hepatic glycogen metabolism is intricately intertwined with systemic lipid metabolism, and fatty liver can also contribute to an increase in hepatic gluconeogenesis [38]. Here, an elevation in glucose and glucose phosphate (GPP) levels was showed in NAFLD, which were downregulated by WEL and DWEL intervention (Figs. 4I and J). The levels of malic acid and succinic acid, both participants in the TCA cycle, were also elevated in NAFLD, indicating the liver's urgent need for energy supply, which was consequently reversed under the influence of WEL and DWEL (Figs. 4K and L). Moreover, spatial metabolomics showed an increase in cholesterol, phospholipids, and fatty acids within NAFLD, such as cholesterol sulfate (CSS), phosphatidylethanolamine (PE)-34:0, phosphatidylserine (PS)-36:2, fatty acid (FA)-16:0, FA-16:1, FA-18:0, FA-20:4, FA-22:5, and FA-22:6. The administration of WEL and DWEL can reverse these lipid disturbances (Figs. 4M–W). However, it is also important to note that not all lipids are regulated with WEL and DWEL uptake, such as phosphatidylglycerol (PG)-36:4, PG-36:5, and PG-38:4 (Fig. S12). Taken together, we discovered that WEL and DWEL can significantly alleviate the metabolic alterations caused by NAFLD.

3.5. Liver-specific transcriptome analysis reveals the differential gene expression patterns and potential functional pathways of WEL and DWEL treatment for NAFLD

To delve into the intricate molecular pathways underlying the therapeutic effects of WEL and DWEL on NAFLD, RNA sequencing was conducted on the zebrafish liver from the control, NAFLD, as well as WEL and DWEL treatment groups. Utilizing the transgenic zebrafish with liver-specific fluorescent proteins expression and visualization characteristics, the zebrafish liver was accurately isolated under a fluorescence microscope, which ensures the exclusive collection of liver samples and the focused transcriptomic analysis. Compared to the control group, a total of 5,587 differentially expressed genes (DEGs) were identified in the NAFLD group induced by TAA, with 2,664 up-regulated and 2,923 down-regulated. And the WEL treatment group exhibited 1,408 DEGs (619 up-regulated and 789 down-regulated) when contrasted with the NAFLD group, whereas the DWEL group and NAFLD group demonstrated 529 DEGs (321 up-regulated and 208 down-regulated, Figs. 5A–C. The stacking histogram of fragments per kilobase of transcript per million mapped reads (FPKM) values presents a high consistency in gene expression patterns within the group (Fig. 5D). It is worth mentioning that there are 71 DEGs overlapped in three experimental comparisons, representing the shared regulation by both WEL and DWEL treatments on TAA-

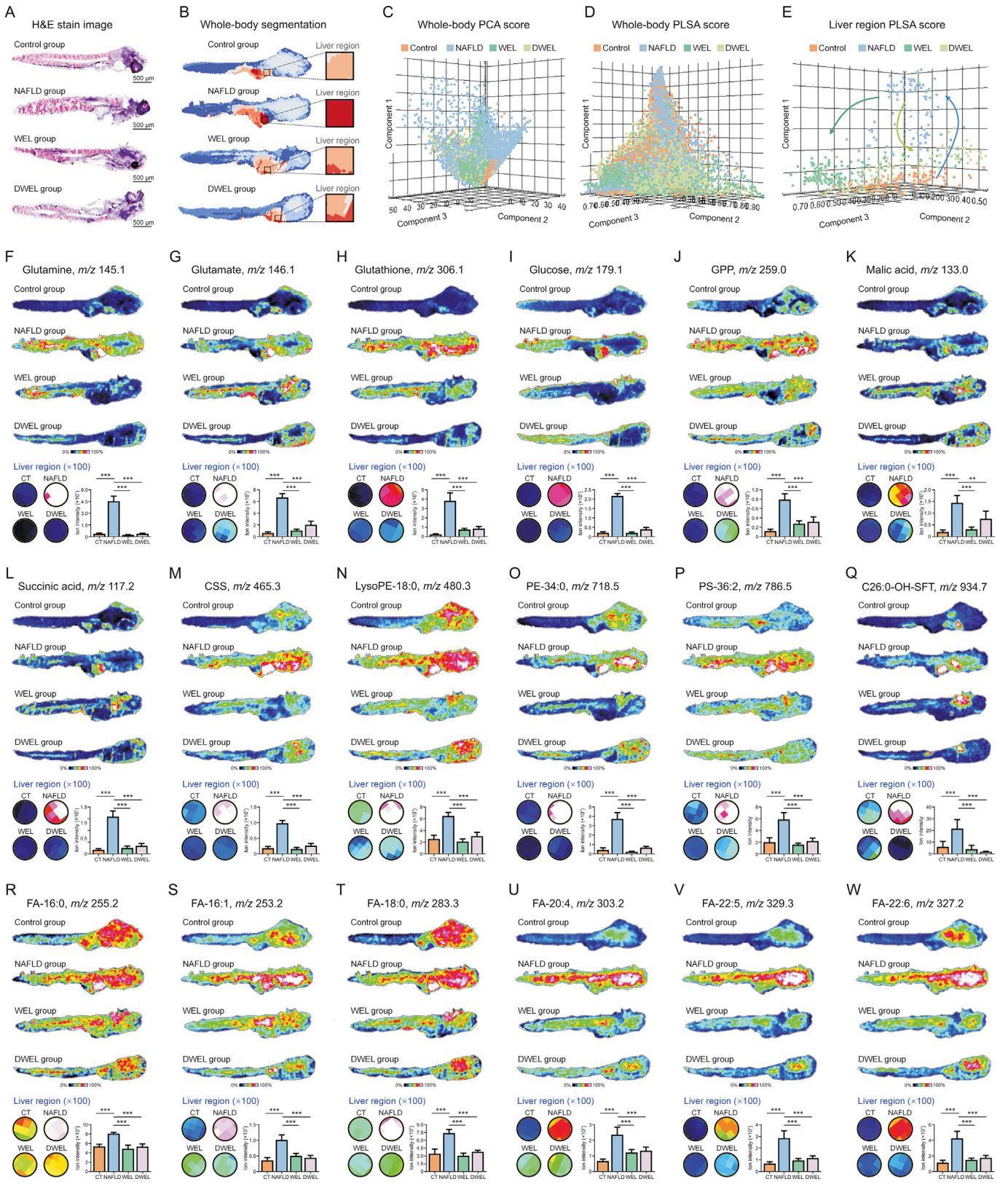

Fig. 4. Spatial metabolomics screened out discriminatory metabolites modulated by wedelolactone (WEL) and demethylwedelolactone (DWEL) on non-alcoholic fatty liver disease (NAFLD). (A) The hematoxylin and eosin (H&E) stain image for model, WEL or DWEL, and normal groups. (B) Metabolite-driven whole-body segmentation analysis based on the matrix-assisted laser desorption/ionization-mass spectrometry imaging (MALDI-MSI) data. (C) Whole-body principal component analysis (PCA). (D) Whole-body probabilistic latent semantic analysis (PLSA). (E) Liver specific PLSA analysis. (F–W) MALDI-MS images and expression levels of altered metabolites in zebrafish whole-body section and liver region. $^{***}P < 0.001$. CT: control; GPP: glucose phosphate; CSS: cholesterol sulfate; lysoPE: lyso-phosphatidylethanolamine; PE: phosphatidylethanolamine; C26:0-OH-SFT: C26:0-OH sulfatide; PS: phosphatidylserine; LysoPC: lyso-phosphatidylcholine; FAs: fatty acids.

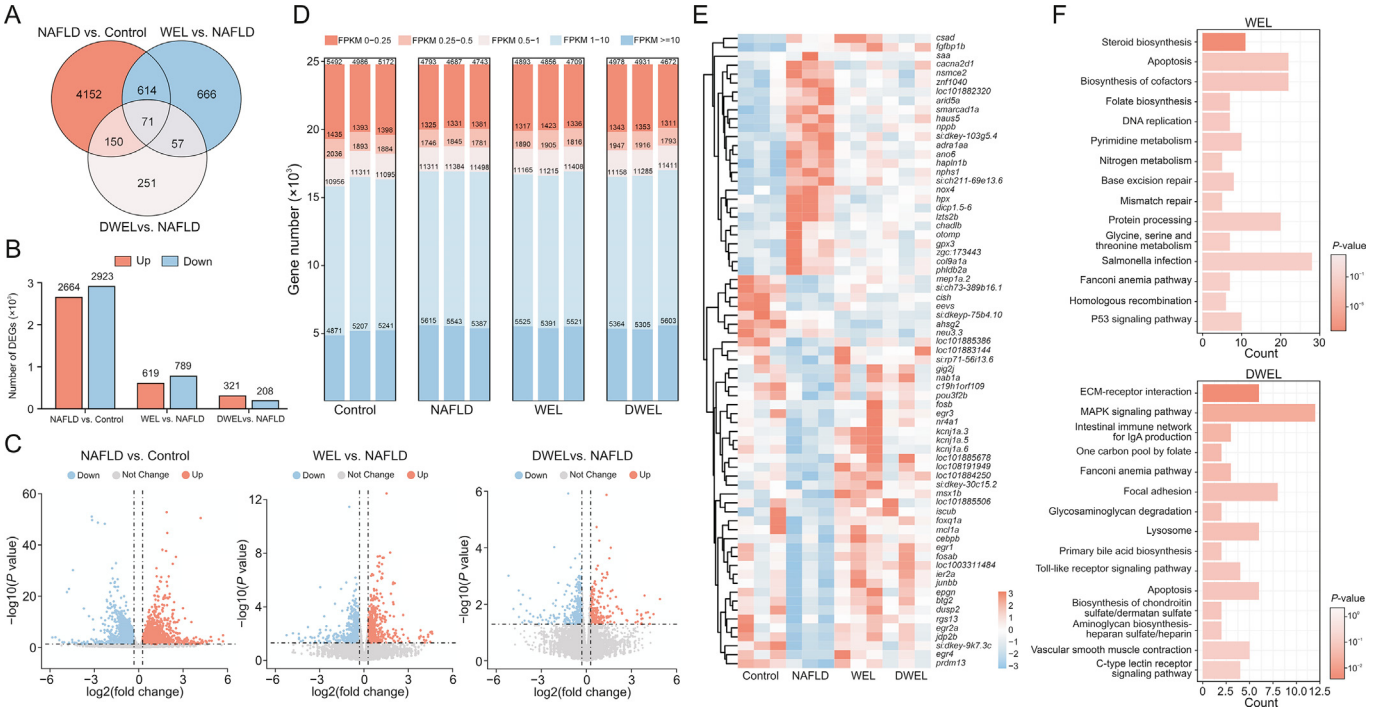

Fig. 5. Wedelolactone (WEL) and demethylwedelolactone (DWEL) extensively altered gene expression patterns in zebrafish liver. (A) Venn diagram analysis of the total differentially expressed genes (DEGs) in three comparisons: non-alcoholic fatty liver disease (NAFLD) group vs. control group, WEL treatment groups vs. NAFLD group and DWEL treatment groups vs. NAFLD group. (B, C) The statistics of DEGs that up-and down-regulated were showed by colored columns (B) and volcano plot (C). (D) Stacking histogram of fragments per kilobase of transcript per million mapped reads (FPKM) values of the genes in each sample. (E) Heatmap of the 71 DEGs overlapped among the three comparisons. (F) Kyoto Encyclopedia of Genes and Genomes (KEGG) pathway enrichment analysis of DEGs in WEL and DWEL treatment groups vs. NAFLD group.

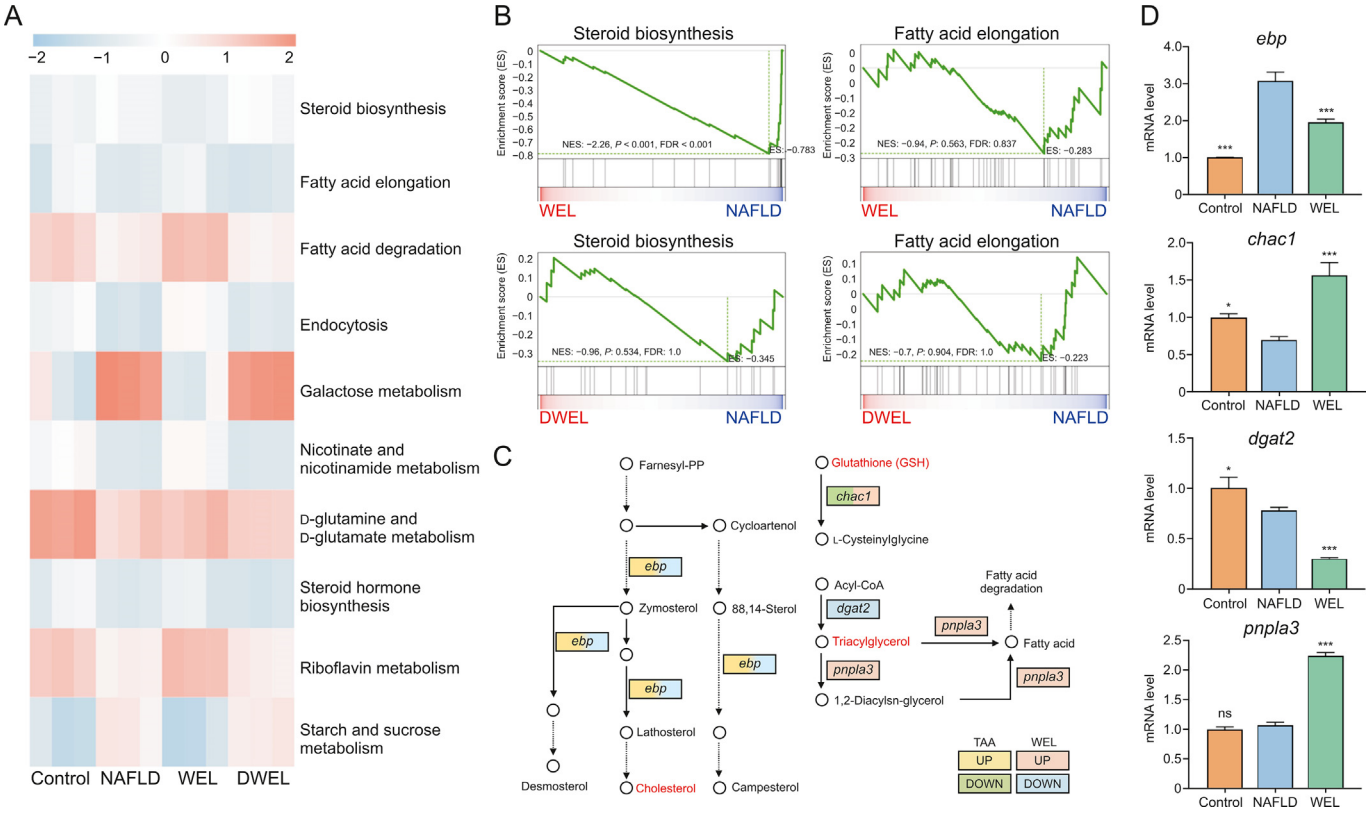

Fig. 6. The integrated analysis of transcriptomic and metabolomic profiles following wedelolactone (WEL) and demethylwedelolactone (DWEL) treatment. (A) Single-sample gene set enrichment analysis (ssGSEA) of the key metabolic pathway across each sample. (B) Gene set enrichment analysis (GSEA) of steroid biosynthesis and fatty acid elongation in WEL and DWEL treatment group vs. non-alcoholic fatty liver disease (NAFLD) group. (C) The biological processes of steroid synthesis, fatty acid metabolism, and glutathione metabolism, and the crucial genes involved. (D) The relative mRNA levels of genes in essential metabolic pathways determined by quantitative real-time PCR (qRT-PCR). Data are presented as mean ± standard deviation (SD) ($n = 10$). $^{*}P < 0.05$, $^{***}P < 0.001$, ns: no significance. NES: normalized enrichment score; FDR: false discovery rate; TAA: thioacetamide; farnesyl-PP: farnesyl pyrophosphate.

induced NAFLD. The clustering heatmap further illustrated the mRNA profiles of these 71 genes clearly segregated WEL and DWEL treatment groups from the NAFLD group (Fig. 5E). Through KEGG enrichment analysis, we found that several biological processes including cellular signaling, energy metabolism, apoptosis, and extracellular matrix interactions were profoundly enriched, indicating that these pathways are shared mechanisms through which WEL and DWEL regulate NAFLD (Fig. S13).

When performing pathway enrichment analysis on DEGs of the WEL vs. NAFLD group and DWEL vs. NAFLD group, distinct differences were observed (Fig. 5F). For the WEL treatment group compared to NAFLD group, the DEGs were predominantly enriched in pathways related to steroid biosynthesis, apoptosis, biosynthesis of cofactors, folate biosynthesis and DNA replication, which are closely associated with maintaining normal hepatic function and reducing fat deposition [39,40]. In contrast, the DEGs between DWEL treatment and NAFLD group were primarily enriched in extracellular matrix (ECM)-receptor interaction, MAPK signaling pathway, intestinal immune network for IgA production, one-carbon pool by folate and Fanconi anemia pathway, etc. These pathways are involved in biological processes such as regulation of signal transduction and immune modulation, indicating that WEL and DWEL exert their effects through different mechanisms on NAFLD.

3.6. The integrated analysis of transcriptomics and metabolomics systematically revealed the differences in the regulation of hepatic metabolism by WEL and DWEL

To gain a deeper insight into the changes in metabolic pathways induced by WEL and DWEL treatments, an integrated analysis combining transcriptomics and metabolomics was conducted. Single-sample gene set enrichment analysis (ssGSEA) revealed significant metabolic dysfunction in NAFLD at the gene level. Interestingly, the majority of these metabolic pathways can be effectively reversed by WEL treatment. However, the effects of DWEL were comparatively limited, indicating a direct correlation between these pathways and the regulatory effects of WEL, rather than DWEL, on NAFLD (Fig. 6A). The metabolic pathways of steroid biosynthesis and fatty acid elongation were then tested by gene set enrichment analysis (GSEA), revealing a downregulation of these pathways with WEL treatment (Fig. 6B). Steroid biosynthesis and fatty acid elongation are highly relevant biological processes to NAFLD, as their dysregulation leads to the accumulation of cholesterol and fatty acids, which are crucial contributors to the lipotoxicity in NAFLD progression [41,42]. These results strongly indicated that WEL exerted its therapeutic effect on NAFLD through regulation of cholesterol and fatty acid metabolism, which is consistent with the results obtained from metabolomics analysis.

We further validated several relevant genes expression through qRT-PCR to strengthen the evidence for the underlying mechanisms of WEL on NAFLD (Figs. 6C and D). Emopamil-binding protein (Ebp), an important enzyme in cholesterol biosynthesis, catalyzes the transformation of delta(8)-sterols into their delta(7)-isomers and is crucial for the steroid homeostasis [43,44]. Its expression can be significantly upregulated in TAA-induced NAFLD and reversely downregulated by WEL treatment. We also verified the markable downregulation of the *dgat2* gene by WEL in the fatty acid metabolism pathway. *Dgat2* is responsible for encoding diacylglycerol O-acyltransferase, which utilizes diacylglycerol and fatty acyl-CoA as substrates to catalyze the formation of triglycerides [45]. The downstream gene *pnpla3*, which is involved in the remodeling of acyl chains in triglycerides [46], was assessed to be upregulated in response to WEL treatment. Additionally, we validated that WEL can reversely regulate the expression of *chac1*, leading to the degradation of glutathione [47], which is consistent with the metabolomic data (Figs. 6D and 4H). In summary, we have demonstrated that WEL and DWEL improve NAFLD through separate mechanisms. Inhibition of steroid biosynthesis and modulation of fatty acid metabolism are important pathways specifically associated with the effects of WEL, not DWEL.

4. Conclusion

Our study provides evidence of the therapeutic effects of WEL and DWEL on NAFLD, and proposes a novel approach combining MSI-based spatial metabolomics with liver-specific transcriptomics to explore their underlying mechanisms. Through spatial metabolomics, the in vivo metabolic pathways of WEL and DWEL in zebrafish as well as the discriminatory endogenous metabolites were comprehensively mapped. Furthermore, transcriptomics analysis revealed the distinct mechanisms of WEL and DWEL on NAFLD, and unveiled the hepatoprotective effects of WEL is mainly associated with the modulation of steroid biosynthesis and fatty acid metabolism. Our findings not only provide a holistic understanding of the impacts of WEL and DWEL on NAFLD, but also emphasize the significance of integrative spatial metabolomics and liver-specific transcriptomics in elucidating the intricate mechanisms for effective intervention.

CRediT author statement

Panpan Chen and **Zihan Zhu**: Methodology, Investigation, Data curation, Writing - Original draft preparation; **Haoyuan Geng** and **Xiaoqing Cui**: Software, Data curation; **Yuhao Han and Lei Wang**: Methodology, Investigation; **Yaqi Zhang and Heng Lu**: Software, Investigation; **Xiao Wang, Yun Zhang** and **Chenglong Sun**: Conceptualization, Resources, Writing - Reviewing and Editing, Supervision.

Declaration of competing interest

The authors declare that there are no conflicts of interest.

Acknowledgments

This study was supported by the National Natural Science Foundation of China (Grant No.: 82273888), Natural Science Foundation of Shandong Province (Grant No.: ZR2022QH257, ZR2020YQ60), Shandong Major Technological Innovation Project (Project No.: 2021CXGC010508), Taishan Scholars Program of Shandong Province (Program Nos.: tsqn202103096, and tsqn202211204), and Shandong Province Science and Technology Small and Medium Enterprises Innovation Ability Enhancement Project (Project No.: 2022TSGC2210).

Appendix A. Supplementary data

Supplementary data to this article can be found online at https://doi.org/10.1016/j.jpha.2023.11.017.

References

[1] J.J. Maher, J.M. Schattenberg, Nonalcoholic fatty liver disease in 2020, Gastroenterology 158 (2020) 1849–1850.
[2] Z. Younossi, Q.M. Anstee, M. Marietti, et al., Global burden of NAFLD and NASH: Trends, predictions, risk factors and prevention, Nat. Rev. Gastroenterol. Hepatol. 15 (2018) 11–20.
[3] M. Eslam, A.J. Sanyal, J. George, MAFLD: A consensus-driven proposed nomenclature for metabolic associated fatty liver disease, Gastroenterology 158 (2020) 1999–2014.el.
[4] P. Burra, C. Becchetti, G. Germani, NAFLD and liver transplantation: Disease burden, current management and future challenges, JHEP Rep. 2 (2020), 100192.

[5] T. Liu, H. Yang, F. Zhuo, et al., Atypical E3 ligase ZFP91 promotes small-molecule-induced E2F2 transcription factor degradation for cancer therapy, EBioMedicine 86 (2022), 104353.
[6] S. Sarma, S. Sockalingam, S. Dash, Obesity as a multisystem disease: Trends in obesity rates and obesity-related complications, Diabetes Obes. Metab. 23 (2021) 3–16.
[7] H. Kitade, G. Chen, Y. Ni, et al., Nonalcoholic fatty liver disease and insulin resistance: New insights and potential new treatments, Nutrients 9 (2017), 387.
[8] Z.M. Younossi, A.B. Koenig, D. Abdelatif, et al., Global epidemiology of nonalcoholic fatty liver disease-Meta-analytic assessment of prevalence, incidence, and outcomes, Hepatol. Baltim. Md. 64 (2016) 73–84.
[9] M.K. Lee, N.R. Ha, H. Yang, et al., Antiproliferative activity of triterpenoids from *Eclipta prostrata* on hepatic stellate cells, Phytomedicine 15 (2008) 775–780.
[10] H. Tang, H. Li, Y. Li, et al., Protective effects of a traditional Chinese herbal formula Jiang-Xian HuGan on Concanavalin A-induced mouse hepatitis via NF-κB and Nrf2 signaling pathways, J. Ethnopharmacol. 217 (2018) 118–125.
[11] K. Rai, K. Yadav, M. Das, et al., Effect of carbon quantum dots derived from extracts of UV-B-exposed *Eclipta alba* on alcohol-induced liver cirrhosis in Golden Hamster, Photochem. Photobiol. Sci. 22 (2023) 1543–1559.
[12] A. Svrlanska, A. Ruhland, M. Marschall, et al., Wedelolactone inhibits human cytomegalovirus replication by targeting distinct steps of the viral replication cycle, Antivir. Res. 174 (2020), 104677.
[13] F. Yuan, J. Chen, P. Sun, et al., Wedelolactone inhibits LPS-induced pro-inflammation via NF-κB pathway in RAW 264.7 cells, J. Biomed. Sci. 20 (2013), 84.
[14] Y. Xia, J. Chen, Y. Cao, et al., Wedelolactone exhibits anti-fibrotic effects on human hepatic stellate cell line LX-2, Eur. J. Pharmacol. 714 (2013) 105–111.
[15] Y. Zhao, L. Peng, L.C. Yang, et al., Wedelolactone regulates lipid metabolism and improves hepatic steatosis partly by AMPK activation and up-regulation of expression of PPARα/LPL and LDLR, PLoS One 10 (2015), e0132720.
[16] W. Goessling, K.C. Sadler, Zebrafish: An important tool for liver disease research, Gastroenterology 149 (2015) 1361–1377.
[17] N. Osmani, J.G. Goetz, Multiscale imaging of metastasis in zebrafish, Trends Cancer 5 (2019) 766–778.
[18] P. Song, N. Jiang, K. Zhang, et al., Ecotoxicological evaluation of zebrafish liver (*Danio rerio*) induced by dibutyl phthalate, J. Hazard. Mater. 425 (2022), 128027.
[19] B.J. Wilkins, M. Pack, Zebrafish models of human liver development and disease, Compr. Physiol. 3 (2013) 1213–1230.
[20] C. Zhang, C. Li, K. Liu, et al., Characterization of Zearalenone-induced hepatotoxicity and its mechanisms by transcriptomics in zebrafish model, Chemosphere 309 (2022), 136637.
[21] Y. Zhang, L. Han, Q. He, et al., A rapid assessment for predicting drug-induced hepatotoxicity using zebrafish, J. Pharmacol. Toxicol. Methods 84 (2017) 102–110.
[22] J. Zhang, L. Qian, C. Wang, et al., UPLC-TOF-MS/MS metabolomics analysis of zebrafish metabolism by spirotetramat, Environ. Pollut. 266 (2020), 115310.
[23] T. He, M. Wang, J. Kong, et al., Integrating network pharmacology and non-targeted metabolomics to explore the common mechanism of *Coptis* Categorized Formula improving T2DM zebrafish, J. Ethnopharmacol. 284 (2022), 114784.
[24] M. Teng, W. Zhu, D. Wang, et al., Metabolomics and transcriptomics reveal the toxicity of difenoconazole to the early life stages of zebrafish (*Danio rerio*), Aquat. Toxicol. 194 (2018) 112–120.
[25] X. Tian, G. Zhang, Z. Zou, et al., Anticancer drug affects metabolomic profiles in multicellular spheroids: Studies using mass spectrometry imaging combined with machine learning, Anal. Chem. 91 (2019) 5802–5809.
[26] Y. Chen, T. Wang, P. Xie, et al., Mass spectrometry imaging revealed alterations of lipid metabolites in multicellular tumor spheroids in response to hydroxychloroquine, Anal. Chim. Acta. 1184 (2021), 339011.
[27] C. Sun, A. Wang, Y. Zhou, et al., Spatially resolved multi-omics highlights cell-specific metabolic remodeling and interactions in gastric cancer, Nat. Commun. 14 (2023), 2692.
[28] C. Sun, T. Li, X. Song, et al., Spatially resolved metabolomics to discover tumor-associated metabolic alterations, Proc. Natl. Acad. Sci. U. S. A. 116 (2019) 52–57.
[29] B. Jin, X. Pang, Q. Zang, et al., Spatiotemporally resolved metabolomics and isotope tracing reveal CNS drug targets, Acta Pharm. Sin. B 13 (2023) 1699–1710.
[30] A.M. Bolger, M. Lohse, B. Usadel, Trimmomatic: A flexible trimmer for Illumina sequence data, Bioinformatics 30 (2014) 2114–2120.
[31] D. Kim, B. Langmead, S.L. Salzberg, HISAT: A fast spliced aligner with low memory requirements, Nat. Methods. 12 (2015) 357–360.
[32] M.I. Love, W. Huber, S. Anders, Moderated estimation of fold change and dispersion for RNA-seq data with DESeq2, Genome Biol. 15 (2014), 550.
[33] S. Hänzelmann, R. Castelo, J. Guinney, GSVA: Gene set variation analysis for microarray and RNA-seq data, BMC Bioinformatics 14 (2013), 7.
[34] K.S. Jones, A.P. Alimov, H.L. Rilo, et al., A high throughput live transparent animal bioassay to identify non-toxic small molecules or genes that regulate vertebrate fat metabolism for obesity drug development, Nutr. Metab. 5 (2008), 23.
[35] H. Ye, S. Ma, Z. Qiu, et al., *Poria cocos* polysaccharides rescue pyroptosis-driven gut vascular barrier disruption in order to alleviates non-alcoholic steatohepatitis, J. Ethnopharmacol. 296 (2022), 115457.
[36] L. Li, X. Huang, J. Peng, et al., Wedelolactone metabolism in rats through regioselective glucuronidation catalyzed by uridine diphosphate-glucuronosyltransferases 1As (UGT1As), Phytomedicine 23 (2016) 340–349.
[37] R.J. DeBerardinis, A. Mancuso, E. Daikhin, et al., Beyond aerobic glycolysis: Transformed cells can engage in glutamine metabolism that exceeds the requirement for protein and nucleotide synthesis, Proc. Natl. Acad. Sci. U. S. A. 104 (2007) 19345–19350.
[38] H.W. Chao, S.W. Chao, H. Lin, et al., Homeostasis of glucose and lipid in non-alcoholic fatty liver disease, Int. J. Mol. Sci. 20 (2019), 298.
[39] N. Alkhouri, C. Carter-Kent, A.E. Feldstein, Apoptosis in nonalcoholic fatty liver disease: diagnostic and therapeutic implications, Expert Rev. Gastroenterol. Hepatol. 5 (2011) 201–212.
[40] J.M. Eng, J.L. Estall, Diet-induced models of non-alcoholic fatty liver disease: Food for thought on sugar, fat, and cholesterol, Cells 10 (2021), 1805.
[41] P. Malhotra, R.K. Gill, S. Saksena, et al., Disturbances in cholesterol homeostasis and non-alcoholic fatty liver diseases, Front. Med. 7 (2020), 467.
[42] D.H. Ipsen, J. Lykkesfeldt, P. Tveden-Nyborg, Molecular mechanisms of hepatic lipid accumulation in non-alcoholic fatty liver disease, Cell. Mol. Life Sci. 75 (2018) 3313–3327.
[43] W.D. Nes, Biosynthesis of cholesterol and other sterols, Chem. Rev. 111 (2011) 6423–6451.
[44] S. Silve, P.H. Dupuy, C. Labit-Lebouteiller, et al., Emopamil-binding protein, a mammalian protein that binds a series of structurally diverse neuroprotective agents, exhibits delta8-delta7 sterol isomerase activity in yeast, J. Biol. Chem. 271 (1996) 22434–22440.
[45] C. Chitraju, T.C. Walther, R.V. Farese, The triglyceride synthesis enzymes DGAT1 and DGAT2 have distinct and overlapping functions in adipocytes, J. Lipid Res. 60 (2019) 1112–1120.
[46] M.A. Mitsche, H.H. Hobbs, J.C. Cohen, Patatin-like phospholipase domain-containing protein 3 promotes transfer of essential fatty acids from triglycerides to phospholipids in hepatic lipid droplets, J. Biol. Chem. 293 (2018) 6958–6968.
[47] R.R. Crawford, E.T. Prescott, C.F. Sylvester, et al., Human CHAC1 protein degrades glutathione, and mRNA induction is regulated by the transcription factors ATF4 and ATF3 and a bipartite ATF/CRE regulatory element, J. Biol. Chem. 290 (2015) 15878–15891.